Title: DOCK3 regulates normal skeletal muscle regeneration and glucose metabolism

Adrienne Samani[1], Muthukumar Karuppasamy[1], Katherine G. English[1], Colin A. Siler[1], Yimin Wang[1], Jeffrey J. Widrick[2], and Matthew S. Alexander[1, 3-7]

[1]Department of Pediatrics, Division of Neurology at the University of Alabama at Birmingham and Children's of Alabama, Birmingham, AL 35294

[2]Division of Genetics and Genomics, Boston Children's Hospital, Boston, MA 02115, USA; Department of Pediatrics, Harvard Medical School, Boston, MA 02115, USA

[3]UAB Center for Exercise Medicine at the University of Alabama at Birmingham, Birmingham, AL, 35294

[4]Department of Genetics at the University of Alabama at Birmingham, Birmingham, AL 35294

[5]UAB Civitan International Research Center (CIRC), at the University of Alabama at Birmingham, Birmingham, AL 35233

[6]UAB Center for Neurodegeneration and Experimental Therapeutics (CNET), Birmingham, AL 35294, USA

[7]Corresponding author

Running Title: DOCK3 is essential for normal muscle function
Keywords: DOCK3, skeletal muscle, regeneration, metabolism
Word Count: 4,871
Character Count: 33,129

Correspondence should be directed to:
Matthew S. Alexander, PhD
University of Alabama at Birmingham and Children's of Alabama
1900 University Blvd. THT 929 Box 96
Birmingham, AL 35294
Email for correspondence: matthewalexander@uabmc.edu

Emails of Authors

adrienne.samani@gmail.com

mkaruppasamy@uabmc.edu

ke111@uab.edu

csiler@uab.edu

ywang@uabmc.edu

jeffrey.widrick@childrens.harvard.edu

matthewalexander@uabmc.edu

Abstract

DOCK (dedicator of cytokinesis) is an 11-member family of typical guanine nucleotide exchange factors (GEFs) expressed in the brain, spinal cord, and skeletal muscle. Several DOCK proteins have been implicated in maintaining several myogenic processes such as fusion. We previously identified DOCK3 as being strongly upregulated in Duchenne muscular dystrophy (DMD), specifically in the skeletal muscles of DMD patients and dystrophic mice. *Dock3* ubiquitous KO mice on the dystrophin-deficient background exacerbated skeletal muscle and cardiac phenotypes. We generated *Dock3* conditional skeletal muscle knockout mice (*Dock3* mKO) to characterize the role of DOCK3 protein exclusively in the adult muscle lineage. *Dock3* mKO mice presented with significant hyperglycemia and increased fat mass, indicating a metabolic role in the maintenance of skeletal muscle health. *Dock3* mKO mice had impaired muscle architecture, reduced locomotor activity, impaired myofiber regeneration, and metabolic dysfunction. We identified a novel DOCK3 interaction with SORBS1 through the C-terminal domain of DOCK3 that may account for its metabolic dysregulation. Together, these findings demonstrate an essential role for DOCK3 in skeletal muscle independent of DOCK3 function in neuronal lineages.

126 **Introduction**

127

128 Skeletal muscle is essential for the body's locomotive function, maintenance of the skeleton
129 structure, and it retains a trademark capacity for repair and regeneration(Chaillou and Lanner
130 2016). As an organ, skeletal muscle plays a major role in the processing and utilization of glucose
131 in response to insulin. Through this mechanism, it is responsible for approximately 80% of
132 postprandial glucose uptake from circulation, making it critical to maintaining metabolic
133 homeostasis at the organismal level(DeFronzo and Tripathy 2009). Many key cell signaling
134 pathways are essential for normal muscle cell regeneration, migration, membrane fusion, repair,
135 and muscle metabolism during growth and development(Sampath, Sampath et al. 2018). Several
136 Rho GTPases function as molecular switches during cell signaling pathways important to the
137 regulation of the F-actin cytoskeleton(Noviello, Kobon et al. 2021). Additional downstream Rho
138 signaling effectors, such as RAC1 and CDC42, have been implicated in myogenic processes
139 including myogenic differentiation, fusion, myoblast proliferation, and are known to influence the
140 regenerative capacity within the skeletal muscle(Samson, Will et al. 2007).

141

142 The *DOCK* gene family is an 11-member class of guanine nucleotide exchange factors capable
143 of influencing multiple pathways involved in cellular fusion, migration, and survival in a myriad of
144 tissue types(Côté and Vuori 2002). Many of these DOCK proteins are highly expressed in the
145 brain, spinal cord, and muscle(Aguet, Anand et al. 2020). Recent studies have demonstrated that
146 DOCK proteins play essential functional roles in important skeletal muscle processes in health
147 and disease(Samani, English et al. 2022). For example, DOCK1 and DOCK5 have been
148 illustrated as crucial players in myoblast fusion(Moore, Parkin et al. 2007, Laurin, Fradet et al.
149 2008). Along those same lines, DOCK3 plays a key role in RAC1 activation and WAVE signaling
150 in neurons and skeletal muscle(Namekata, Enokido et al. 2004, Namekata, Harada et al. 2010,

151 Helbig, Mroske et al. 2017). Patients with loss-of-function *DOCK3* variants present with a variety
152 of developmental disorders such as intellectual disability, developmental delay, ataxia, and
153 muscle hypotonia(Helbig, Mroske et al. 2017, Iwata-Otsubo, Ritter et al. 2018).

154

155 Previously, we identified DOCK3 as a dosage-sensitive biomarker of DMD in which disease
156 severity correlated with increased DOCK3 expression in the skeletal muscles of affected patients
157 and dystrophic *mdx*^{5cv} mice(Reid, Wang et al. 2020). Interestingly, the adult skeletal muscle of the
158 ubiquitous *Dock3* KO mice showed a reduction in myofiber diameter and overall structure,
159 reduced muscle mass, and metabolic dysfunction. DOCK3 is expressed in both the central
160 nervous system and in skeletal muscle, thus we sought to understand the role of DOCK3
161 exclusively in the skeletal muscle by generating a skeletal muscle-specific conditional mouse
162 knockout of *Dock3* within the myofiber. We hypothesized that a muscle-specific loss of DOCK3
163 would disrupt major myogenic processes and protein-protein interactions, subsequently
164 undermining muscle regeneration, metabolism, and overall muscle function. We generated a
165 muscle-specific mouse model (henceforth referred to as *Dock3* mKO) to understand the role of
166 DOCK3 in overall muscle health. We evaluated *Dock3* mKO mouse models and found mild
167 disruptions in muscle integrity and function using activity tracking, but no evidence of contractile
168 deficits using *ex vivo* functional assays. We evaluated the role of DOCK3 in muscle repair and
169 showed an impairment in the skeletal muscle's capacity to repair in the *Dock3* mKO mice following
170 a cardiotoxin-induced injury. Finally, we evaluated the impact of DOCK3 on glucose metabolism
171 via its activation of the GLUT4 transporter and identified a novel protein-protein interaction with
172 the insulin adaptor protein Sorbin and SH3 domain containing 1 (SORBS1). We demonstrated that DOCK3
173 is essential for normal skeletal muscle regeneration and metabolic regulation within the skeletal muscle.

174

175 **Materials and Methods**

176 *Animals*

177 *Dock3* conditional knockout mice were generated commercially (Cyagen; Santa Clara, CA).
178 These mice were generated using a CRISPR-Cas9 approach to generate an out-of-frame *Dock3*
179 deficient mouse upon *Cre*-mediated recombination by excision of exons 8 and 9 of the mouse
180 *Dock3* transcript (NCBI Reference Sequence: NM_153413). Guide RNAs (gRNAs) targeting the
181 intronic regions flanking mouse *Dock3* exons 8 and 9 were used along with a homologous
182 recombination vector were injected into wild type *C57BL/6* mouse embryos (Taconic Biosciences;
183 Germantown, NY) to generate Dock3 conditional knockout mice (*Dock3*$^{fl/fl}$). The targeting
184 homologous recombination vector contained loxP sites flanking mouse *Dock3* exons 8 and 9 and
185 was co-injected with the gRNAs and Cas9 mRNA. F_0 founder mice were identified by PCR
186 followed by sequence analysis and were then backcrossed to wild type mice to test germline
187 transmission and F_1 animal generation. PCR oligonucleotide primers used to genotype the
188 genomic tail DNA from isolated biopsies from the loxP sites in the *Dock3* conditional mice were
189 F: 5'-GAGATGCTGATTTCACTGTCTAGC-3' and R: 5'-CTCTTATCACTGGCTGAAACTACA-3'.
190 PCR primers for the *Cre recombinase* transgene used were Forward: 5'-
191 GAACGCACTGATTTCGACCA-3' Reverse: 5'-GCTAACCAGCGTTTTCGTTC-3. Skeletal
192 myofiber tamoxifen-inducible mice were purchased from Jackson Labs (Bar Harbor, ME) Human
193 Skeletal-Actin-MerCreMer (*HSA-MCM*) mice (Jackson Labs; Bar Harbor, ME; stock# 025750) and
194 WT (*C57BL/6J*; stock# 000664) were maintained in our animal colony under pathogen-free
195 standard housing conditions. *Dock3* ubiquitous KO mice (Jackson Labs; stock# 033736) were
196 originally obtained from the laboratory of Dr. David Shubert (Salk Institute) and have been
197 previously described (10). The *mdx*^{5cv} (Jackson Labs; stock# 002379) mice were originally
198 obtained from Jackson Labs. All mice were maintained on the *C57BL/6J* strain background. All
199 mouse strains were maintained under standard housing and feeding conditions with the University
200 of Alabama at Birmingham Animal Resources Facility under pathogen-free, sterile conditions

201 under animal protocol number 21393. Mice were all fed a diet consisting of the
202 Teklad Global Rodent Diets (Envigo; Indianapolis, IN) with *ad libitum* access to food and water.

203

204 *GLUT4-transfection*

205 WT and *Dock3* KO primary mouse muscle cells were harvested from the ubiquitous *Dock3* KO
206 mice as previously described(Chen, Peto et al. 2009). Primary mouse myoblasts were grown in
207 Skeletal Muscle Cell Growth Medium (Promocell Cat# C-23060; Heidelberg, Germany) with 20%
208 FBS (ThermoFisher Scientific; Waltham, MA; Cat# 16140071), and incubated at 37°C using a
209 standard primary muscle cell isolation protocol(Gharaibeh, Lu et al. 2008). Muscle cells were
210 plated in a 6-well gelatin coated plate at 50,000 cells/well. Muscle cells were then transfected with
211 a pLenti-myc-GLUT4-mCherry (Addgene; Watertown, MA; stock # 64049) for 48 hours and the
212 GLUT4 localization assay was performed as previously described(Lim, Bi et al. 2015).

213

214 *Mouse activity tracking*

215 Mouse activity locomotor measurements were performed as previously described(Reid, Wang et
216 al. 2020). Twenty-four hours prior to experiment termination and tissue harvest, mice were
217 analyzed for locomotive activity using the Ethovision XT software platform (Noldus; Leesburg,
218 VA) with isolated individual chambers that recorded motion from mouse head to tail. Mice were
219 acclimated to the room and open-field chambers one day prior to activity and were given a five
220 minute additional adaptation period prior to activity recording. Mouse activity was recorded for six
221 minutes with no external stimulation.

222

223 *Myofiber diameter calculations*

224 The cross-sectional area (CSA) of the myofibers within the skeletal muscle sections was
225 calculated by quantifying the myofiber areas using a previously described protocol(Mula, Lee et
226 al. 2013). Approximately 600 TA myofibers were counted and CSA (μm^2) was measured via
227 several overlapping H&E microscopy images of each section and quantified using Fiji
228 software(Schindelin, Arganda-Carreras et al. 2012).

229

230 *DEXA Quantitative Magnetic Resonance (QMR) imaging*

231 Evaluation of body composition comprising of both fat and lean tissue mass *in vivo* was performed
232 on 4-month-old male *Dock3*$^{fl/fl}$ and *Dock3* mKO mice (10 mice/genotype) using the EchoMRI™ 3-
233 in-1 composition analyzer (software version 2016, Echo Medical; Houston, TX). Individual fat and
234 lean mass measurements were recorded in grams (g) and were analyzed using student's t-test,
235 two-tailed between *Dock3*$^{fl/fl}$ and *Dock3* mKO mice.

236

237 *Cardiotoxin-induced skeletal muscle injury*

238 *Dock3* mKO and *Dock3*$^{fl/fl}$ mice were injected in their TA skeletal muscles with 40 µl of cardiotoxin
239 (MilliporeSigma; Cat# 217503) at a 10 µM concentration. The contralateral TA muscle was used
240 as a sham control injection with 1x phosphate-buffered saline (ThermoFisher Scientific; Cat#
241 10010049). Seven days following injections, mice were euthanized, and their TA skeletal muscles
242 were slow-frozen in Scigen TissuePlus O.C.T. Compound (Fisher Scientific; Hampton, NH Cat#
243 23-730-571) for histological analysis and snap frozen in liquid nitrogen for molecular analysis.

244

245 *Immunofluorescence and immunohistochemistry*

246 Mouse skeletal muscles were cryo-frozen in Scigen TissuePlus O.C.T. Compound using an
247 isopentane (FisherScientific; Cat# AC397221000) and liquid nitrogen bath as unfixed tissues.
248 Blocks were later cut on a cryostat into 7-10 µm sections and placed on Fisherbrand Tissue Path
249 Superfrost Plus Gold slides (Fisher Scientific; Cat# FT4981gplus). H&E staining was performed
250 as previously described(Beedle 2016). For immunofluorescent staining, slides were blocked for
251 one hour in 10% goat serum and incubated for one hour at room temperature using a M.O.M kit
252 (Vector Labs Cat# BMK-2202; Newark, CA).

253

254 *Western blotting*

255 Protein lysates were obtained by homogenizing tissues in M-PER lysis buffer (ThermoFisher;
256 Cat# 78501) with 1x Complete Mini EDTA-free protease inhibitor cocktail tablets (Roche Applied
257 Sciences; Cat# 04693159001; Penzburg Germany). Protein lysates were quantified using a
258 Pierce BCA Protein Assay Kit (ThermoFisher Cat# 23225). Unless stated otherwise, 50 µg of
259 whole protein lysate was used for all immunoblots and resolved on 4-20% Mini-PROTEAN TGX
260 Precast Protein gels (BioRad; Cat# 4561094). Protein samples were transferred to 0.2 µm PDVF
261 membranes (ThermoFisher; Cat# LC2002), blocked in 0.1x TBS-Tween in 5% BSA for one hour,
262 and then gently incubated overnight with primary antibody on a rocker at 4°C. Membranes were
263 washed in 0.1% TBS-tween four times at 10-minute intervals before being incubated with
264 secondary antibodies (either mouse or rabbit IgG) conjugated to HRP for one hour at room
265 temperature with gentle agitation. Following another three washes for 15 minute intervals at room
266 temperature, membranes were then treated with RapidStep ECL Reagent (MilliporeSigma; Cat#
267 345818-100 ml).

268

269 *Real-time quantitative PCR*

270 Total RNA was extracted using a miRVana (ThermoFisher, Cat# AM1560) kit while following the
271 manufacturer's protocol. One microgram of total RNA was reverse transcribed using the Taqman
272 Reverse Transcription kit (Applied Biosystems; Cat# N8080234; Waltham, MA) following the
273 manufacturer's protocol. TaqMan assay probes were all purchased from ThermoFisher
274 corresponding to each individual transcript. Quantitative PCR (qPCR) TaqMan reactions were
275 performed using TaqMan Universal PCR Master Mix (Applied Biosystems; Cat# 4304437).
276 Relative expression values were calculated using the manufacturer's software and further
277 confirmed using the $2^{-\Delta\Delta}$Ct method.

278

279 *Glucose and insulin tolerance tests*

280 Mice were fasted for eight hours prior to afternoon administration of a bolus of D-glucose
281 (MilliporeSigma; Cat# G8270). Mice were given an intraperitoneal injection at a concentration of
282 3 mg/gram of mouse bodyweight. Blood glucose was measured on a commercially obtained
283 glucometer (Nipro Diagnostics Inc.; Southampton, UK) using 10 µl of whole serum from tail
284 bleeds. For the insulin tolerance tests, the mice were fasted for five hours prior to afternoon
285 administration of a bolus of human insulin (MilliporeSigma; Cat# 1342106). Mice were given an
286 intraperitoneal injection at a concentration of 3 mg/gram of mouse bodyweight. Blood glucose
287 was measured on a commercially obtained glucometer using 10 µl of whole serum from tail
288 bleeds.

289

290 *Yeast-2-Hybrid*

291 The GAL4-based yeast two hybrid system was used to detect the interaction between
292 recombinant DOCK3 and SORBS1 domains. The bait and prey are expressed as fusion domain
293 constructs to the GAL4 DNA binding domain and GAL4 activation plasmids. Inoculations were

294 then transferred to a 500 mL flask containing 300 mL yeast peptone dextrose (YPD) broth
295 (ThermoFisher Scientific; Cat# A1374501) and incubated at 30°C for 16-18 hours with shaking at
296 230 rpm. Cultures were incubated at 30°C for 16-18 hours with shaking at 230 rpm in an overnight
297 culture flask containing 300 ml of YPD. Cultures were harvested in 50 ml tubes and centrifuged
298 at 1000 x g for five minutes at room temperature. Cell pellets were resuspended in distilled water
299 and again centrifuged at 1000 x g for five minutes. Pellets were then re-suspended in 1.5 ml
300 freshly prepared, sterile 1X TE/1X LiAc solution. Approximately 0.1 µg of plasmid DNA and 0.1
301 mg of carrier DNA was added to a 1.5 mL tube and mixed. Approximately 0.1 ml of yeast
302 competent cells were then added to each tube and vortexed until well mixed, heat shocked for
303 five minutes in a 42°C water bath, and chilled on ice for 2 minutes. Yeast cultures were then
304 centrifuged for five seconds at 12,000 x g and resuspended in 0.5 µL sterile TE buffer. The cells
305 were plated at 100 µL each on SD/-LEU/-Trp selective transformant agar plates and incubated at
306 30°C until colonies appeared the next morning.

307

308 *Co-immunoprecipitation (co-IP)*

309 Protein constructs were expressed in HEK293T cells using Lipofectamine 2000-mediated
310 (Invitrogen, Catalog #11668030; Waltham, MA) plasmid transfection. Expression constructs were
311 subcloned into Vitality hrGFP mammalian expression vectors (Agilent Technologies; Santa Clara,
312 CA; Cat# 240031 and #240032) using standard PCR cloning techniques. HEK293T cells were
313 collected two days post-transfection and lysed in lysis buffer that contained 50 mM Tris-HCl (pH
314 7.4), 150 mM NaCl, 1 mM EDTA, 1% Triton X-100, and 1:100 Protease/Phosphatase Inhibitor
315 Cocktail (Cell Signaling Technology; Danvers, MA). Cells were then homogenized using an Omni
316 Bead Rupter 12 (Perkin Elmer; Kennesaw, GA). Protein lysates were then incubated on ice for
317 thirty minutes. Lysates were spun down at 10000 x g for ten minutes, and the supernatant was
318 collected for co-IP. Protein levels were quantified using the BCA Kit and normalized (Pierce

319 Protein Biology, Rockford, IL, USA). Approximately 5% of total protein lysate was set aside as the
320 input fraction. Laemmli Buffer plus β-mercaptoethanol was then added to these samples and one
321 mg of total protein lysate was used per co-IP reaction. Approximately 0.5 mg of mouse IgG control
322 (ThermoFisher, Catalog # MA1-213) was used for the control reaction. Co-IP reactions were
323 rotated overnight at 4°C with 100 µl of SureBeads Protein G Magnetic Beads (BioRad; Catalog#
324 1614013; Hercules, CA). The bead lysates were washed five times in the co-IP buffer using a
325 DynaMag Magnet (ThermoFisher) to pull down the complexes. After this, Laemmli Buffer plus β-
326 mercaptoethanol was added to the beads, which were boiled for five minutes at 100°C. All co-IP
327 reactions were probed using standard western immunoblotting techniques described above. The
328 rabbit DOCK3 (ThermoFisher; Cat# PIPA5100485) and mouse SORBS1 (Sigma-Aldrich; Catalog
329 #SAB4200599; St. Louis, MO) antibodies were used for verifying immunoprecipitation reactions
330 via western immunoblotting. Anti-FLAG M2 magnetic beads (MilliporeSigma; Catalog #M8823)
331 and anti-FLAG M2 monoclonal antibody (MilliporeSigma; Catalog #F1804) were used for co-IP
332 and western immunoblotting reactions. A µMACS HA magnetic bead isolation kit (Miltenyi Biotec;
333 Catalog# 130-091-122) and anti-HA rabbit monoclonal (GenScript; Catalog #A01963) were also
334 used for co-IP and western immunoblotting reactions.

335

336 *GST pulldown assay*

337 Recombinant SORBS1 protein (Abcam; Cambridge, UK) was incubated with recombinant GST-
338 DOCK3-PXXP or GST alone plasmids (constructs cloned into pGEX-6P-1 plasmid; GE
339 Healthcare; Chicago, IL) in GST reaction buffer (250 mM Tris-HCl at pH 7.4, 500 mM NaCl, 25
340 mM $MgCl_2$, 5 mM dithiothreitol, 0.5 mM EGTA and 20 mM freshly prepared ATP) for one hour at
341 4°C on a rotator. Pierce Glutathione Magnetic Agarose Beads (ThermoFisher; Cat# 78602) were
342 then suspended in the GST reaction buffer and added to the reaction mixture for one hour at 4°C
343 with gentle rotation. The beads were then washed four times in reaction buffer using a DynaMag

344 magnet. Laemmli Buffer plus β-mercaptoethanol was added to these samples, which were then
345 boiled for five minutes at 100°C. GST pulldown was verified via immunoblot against the GST
346 epitope (anti-GST; rabbit polyclonal; Abcam; Cat# ab9085).

347

348 *Muscle physiological function assays*

349 EDL muscles were dissected from anesthetized mice and studied in a phosphate buffer
350 equilibrated with 95% O_2, 5% CO_2 (35 °C). Contractions were produced using a 150 ms,
351 supramaximal stimulus train (200 μs pulses) with the muscle held at its optimal length (L_o) for
352 tetanic tension. Force was normalized to physiological cross-sectional area as previously
353 described (Huntoon et al. 2018). Each muscle was studied at stimulation frequencies ranging
354 from 30 to 300 Hz (peak force). Fixed-end force values were expressed relative to peak force and
355 fit by a sigmoid curve as previously described(Huntoon, Widrick et al. 2018). Changes in the
356 relationships were evaluated by differences in the inflection point (K, measured in Hz) and slope
357 (H, unitless). Muscles were then subjected to a high active strain protocol consisting of the
358 following sequence: one fix-end trial, 5 lengthening (eccentric) trials, and two fixed-end trials. The
359 fixed-end trials were as described above. The lengthening trials consisted of an initial fixed-end
360 contraction that allowed the muscle to rise to peak force (100 ms duration), followed by a constant
361 velocity stretch at 4 fiber lengths/s (50 mms duration) to a final length of 120% L_o. For the high-
362 strain protocol, force was evaluated at 95 ms of stimulation for both fixed-end and lengthening
363 trials.

364

365 *Statistical analyses*

366 Unless otherwise described, a two-tailed student's t-test was performed for all single comparisons
367 and either a one-way or two-way analysis of variance (ANOVA) with Tukey's post-hoc honest

368 significant difference (HSD) was performed for all multiple comparisons. GraphPad Prism version
369 9 software (Graphpad Software; San Diego, CA) was used for all statistical analyses. An *a priori*
370 hypothesis of *p< 0.05, **p<0.01, ***p<0.001, and ****p< 0.0001 was used for all reported data
371 analyses. All graphs were represented as mean +/- SEM.

372

373 **Results**

374 ***Generation of a muscle-specific Dock3 knockout mouse***

375 As DOCK3 protein is expressed both within the motor neuron and in the skeletal muscle, we
376 generated a conditional mouse model to differentiate the role of the *Dock3* gene exclusively in
377 skeletal muscle. We investigated the specific function of *Dock3* in the myofiber by evaluating
378 *Dock3*-deficient mice in which exons 8 and 9 of the *Dock3* gene locus is flanked with loxP sites in
379 the intronic regions (**Figure 1A**). Upon mating with the mouse model expressing tamoxifen-
380 inducible *Cre recombinase* driven by the human-skeletal actin promoter (*HSA-MerCre-Mer*; *HSA-*
381 *MCM*), the mice will conditionally ablate *Dock3* expression upon tamoxifen administration in the
382 skeletal myofibers **(Figure 1A).** Genotyping and western blot analyses of *Dock3* expression in the
383 tissue extracts of brain and the tibialis anterior (TA) from control and *Dock3* ubiquitous KO mice
384 confirmed the ablation of *Dock3* from the myofiber. The *Dock3*$^{fl/fl}$*:HSA-MerCreMer* (henceforth
385 referred to as *Dock3* mKO*)* mice showed the deletion of *Dock3* expression in tissue extracts from
386 the TA lysates, but not the brain, confirming the tissue-specific deletion of *Dock3* from the myofiber
387 (**Figures 1B, 1D, and 1E**).

388

389 ***Dock3 mKO mice have disrupted skeletal muscle histology and locomotor activity***

390 To evaluate the consequences of *Dock3* skeletal muscle ablation, we first analyzed the muscle
391 architecture and morphology of isolated TA muscle fibers of 4-month-old *Dock3* mKO mice
392 compared to *Dock3*$^{fl/fl}$ controls **(Figure 2A)**. We observed a decrease in myofiber cross-sectional
393 area (CSA) and noted smaller myofibers grouped together throughout the *Dock3* mKO muscles
394 (**Figure 2B**). We did not observe a change in centralized myonuclei. However, we did observe
395 muscle fiber atrophy reflected by increased frequency of smaller myofibers in *Dock3* mKO mice
396 compared to *Dock3*$^{fl/fl}$ controls. We sought to characterize how the disruption of *Dock3* in the
397 skeletal muscle would impact overall locomotive function by using open field activity tracking to
398 record activity levels in adult mice (**Figure 3A**). *Dock3* mKO mice demonstrated significantly
399 decreased distance traveled and average velocity compared with controls, indicating a reduction
400 in basal locomotor function (**Figures 3B-D**). These findings are consistent with a decrease in
401 locomotor function previously observed in adult ubiquitous *Dock3* KO mice. Interestingly, when
402 we conducted several functional assays on extensor digitorium longus (EDL) muscles isolated
403 from *Dock3* mKO and *Dock3*$^{fl/fl}$ mice we found no significant changes in the muscle's contractile
404 properties (**Figures 3E-3J**). This included the relationship between stimulus frequency and force
405 (**Figures 3E-G**), absolute peak force (**Figure 3G**), force normalized to the muscle's physiological
406 cross-sectional area (**Figure 3I**), and in the muscles resistance to eccentric contractions (**Figures
407 3J and 3K**). Therefore, we concluded that loss of *Dock3* in the myofiber reduces basal activity
408 independent of undermining the overall contractility and structural integrity of the skeletal muscle.

409

410 ***Loss of Dock3 at the myofiber inhibits myogenic regeneration after cardiotoxin injury***

411 Previously, we isolated primary myoblasts isolated from *Dock3* KO muscle which exhibited
412 impaired regeneration and fusion. We sought to determine if this phenomenon was recapitulated
413 in our *Dock3* mKO mice and the degree to which muscle regeneration is impacted by the loss of
414 muscle DOCK3 expression **(Figure 4A).** We performed an intramuscular injection of cardiotoxin

415 in our *Dock3* mKO mice to induce a skeletal muscle injury into the right TA muscle while using
416 the left as a contralateral control receiving a sham injection of phosphate buffered saline (PBS)
417 to evaluate the role of DOCK3 in muscle regeneration. Mice were sacrificed at 7 days post-injury
418 and evaluated via histological analysis with hematoxylin and eosin (H&E) and Masson's trichrome
419 to assess myofiber cross-sectional area, myonuclei position, and fibrosis within the muscle. We
420 observed that the *Dock3* mKO mice had increased fibrosis when compared to the control *Dock3*$^{fl/fl}$
421 **(Figures 4B and 4C)**. We also quantified increased levels of centralized myonuclei in the *Dock3*
422 mKO mice (**Figure 4C**). We repeated the study for 14 days post cardiotoxin TA muscle injury and
423 observed similarly impaired muscle regeneration in the *Dock3* mKO mice as seen in the *Dock3*
424 global KO mice (**Figure 4D**). These findings were consistent with the high levels of centralized
425 myonuclei and fibrotic areas observed, indicating a delay in regeneration in the skeletal muscle
426 of *Dock3* mKO mice and emphasizing the importance of DOCK3 in skeletal muscle.

427

428 ***Adult Dock3 mKO mice have abnormal skeletal muscle mass and metabolism***

429 We previously demonstrated that *Dock3* ubiquitous KO mice were glucose intolerant and had
430 decreased weights due to decreased muscle mass. Thus, we sought to understand if the loss of
431 *Dock3* in the skeletal muscle would impact whole-body metabolism. Quantitative magnetic
432 resonance (QMR) imagining of adult *Dock3* mKO mice revealed increased body weight compared
433 to *Dock3*$^{fl/fl}$ aged-matched controls **(Figure 5A)**. Conversely, *Dock3* mKO mice had significantly
434 increased fat mass compared to *Dock3*$^{fl/fl}$ aged-matched controls (**Figure 5B).** No detectable
435 changes in skeletal muscle lean mass were observed in the *Dock3* mKO mice **(Figure 5C)**. Being
436 that DOCK3 is known to activate Rho GTPases such as RAC1, a critical regulator of insulin and
437 glucose signaling pathways in skeletal muscle. We measured the ability of the *Dock3* mKO mice
438 to respond to a glucose challenge via a glucose tolerance test (GTT). GTT tests revealed no
439 significant changes in glucose processing in the muscle **(Figure 5D).** However, insulin tolerance

440 tests (ITT) conducted on *Dock3* mKO mice revealed whole body hyperglycemia and insulin
441 resistance **(Figure 5E).** We analyzed the role of DOCK3 in glucose processing within the muscle
442 by isolating primary *Dock3* KO myoblasts and infecting with lentiviral GLUT4-RFP(Wang, Khayat
443 et al. 1998). Upon insulin stimulation, we observed reduced GLUT4 translocation in the *Dock3*
444 KO myoblasts, which supports a defect in glucose uptake and/or processing within the skeletal
445 muscle (**Figure 5F**). These findings reveal DOCK3 to be a critical regulator of metabolism in the
446 skeletal muscle and that loss of DOCK3 expression in the myofiber undermines important
447 metabolic functioning and insulin processing in the skeletal muscle.

448

449 ***DOCK3 interacts with insulin signaling protein, Sorbin and SH3 domain-containing 1***
450 ***(SORBS1)***

451 Due to the increased fat mass, body weight, and hyperglycemia observed in the *Dock3* mKO
452 mice, we explored what potential protein-protein interactions DOCK3 may be involved with
453 regarding glucose uptake. We conducted a yeast two-hybrid neuromuscular cDNA library screen
454 using the C-terminal domain of human DOCK3 protein to identify novel DOCK3 protein
455 interactions (**Figure 6A**). We identified the insulin adaptor protein, SORBS1 as directly interacting
456 with the C-terminal domain of DOCK3 and confirmed the interaction via secondary yeast amino
457 acid growth selection confirmation (**Figure 6B and Figure 6C**). SORBS1, also called Cbl-
458 Associated Protein (CAP), is a known insulin adaptor protein whose subcellular localization is
459 essential to downstream insulin signaling events and has been implicated as a secondary
460 signaling pathway critical to insulin-mediated glucose uptake(Baumann, Ribon et al. 2000). To
461 determine which domains of each protein were critical to their interaction, we conducted a GST-
462 pulldown assay in HEK293T cells overexpressing DOCK3 and SORBS1. The proline rich motif
463 (PXXP) of DOCK3 and the SH3 domains of SORBS1 were identified as the main sites of the
464 DOCK3-SORBS1 protein interaction (**Figures 6D-6F**). Following these results, we sought to map

465 out which functional domains were critical to the DOCK3-SORBS1 interaction. Overexpression
466 constructs containing full length and deletion of key conserved protein functional domains of
467 DOCK3 and constructs deleting each of the SH3 domains of SORBS1 were generated **(Figure**
468 **7A).** Co-immunoprecipitation confirmed that all three SH3 domains on SORBS1 were essential
469 for the DOCK3-SORBS1 interaction **(Figure 7B).** This protein-protein interaction between DOCK3
470 and SORBS1 was further validated in human primary myotubes **(Figures 7C-7D).** These results
471 identified the DOCK3-SORBS1 interaction as a potential novel source of metabolic regulation that
472 may modulate glucose and insulin signaling in skeletal muscle.

473

474 **Discussion**

475 DOCK3 is a guanine-nucleotide exchange factor whose downstream activation of Rho GTPases
476 impacts a number of pathways that influence cell migration, insulin signaling, and pathways
477 regulating muscle mass(Bryan, Li et al. 2005, Chiu, Jensen et al. 2011). Our previous work
478 identified DOCK3 as an important biomarker and dosage-sensitive regulator of Duchenne
479 muscular dystrophy(Reid, Wang et al. 2020). Here, we identified the muscle-specific role of
480 DOCK3 in the myofiber, apart from its role in the motor neuron, and how its expression is
481 expression is critical to normal muscle function, regeneration and glucose processing within the
482 muscle. Furthermore, using a yeast-two-hybrid screen we identified a novel protein-protein
483 interaction with SORBS1, a key glucose and insulin signaling factor that may yield clues into
484 DOCK3's regulation of skeletal muscle metabolic function via glucose and insulin signaling
485 pathways.

486

487 Additional questions remain as DOCK3 has been shown to interact with RAC1, another key
488 regulator of glucose processing in skeletal muscle which may also explain our observed

489 phenotypes in the *Dock3* mKO mice(Sylow, Jensen et al. 2013, Li, Mi et al. 2016, Raun, Ali et al.
490 2018). Our observation of impaired skeletal muscle regeneration following cardiotoxin injury in the
491 *Dock3* mKO mice suggests that DOCK3 may play roles in muscle regeneration even though it is
492 not expressed in the muscle satellite or stem cells. DOCK3 has been shown to play key roles in
493 cell migration, actin polymerization, and regulates key signaling pathways such as WAVE which
494 may explain the observed impaired regeneration in the *Dock3* mKO mice(Namekata, Harada et
495 al. 2010). The observation of *Dock3* mKO mice having whole-body hyperglycemia and insulin
496 resistance could be a result of the disruption of the DOCK3-SORBS1 interaction. SORBS1 is part
497 of a small family of adaptor proteins that is known to regulate numerous cellular processes
498 including cell adhesion, cytoskeletal formation, and is required for insulin-stimulated glucose
499 transport(Mandai, Nakanishi et al. 1999). A number of studies suggest that genetic variations in
500 SORBS1 could be associated with human disorders such as obesity, diabetes, and insulin
501 resistance(Baumann, Ribon et al. 2000, Lesniewski, Hosch et al. 2007, Chang, Wang et al. 2018).
502 *Dock3* mKO mice showed significantly increased fat mass and body mass, without any impact on
503 lean mass. The novel interaction between DOCK3 and SORBS1 implies that DOCK3 plays a
504 significant metabolic role in the muscle, specifically involving regulation of insulin-mediated
505 glucose uptake. Further studies are warranted to dissect DOCK3's additional roles in other
506 lineages using a conditional approach.

507

508 **Conflict of Interest Statement**

509 The authors declare no conflicts of interest.

510

511 **Author Contributions**

512 A. Samani, M. Karuppasamy, K. English, C. Siler, Y. Wang, and J. Widrick all performed
513 experiments related to the project and analyzed the data. A.Samani, M. Karuppasamy, K. English,
514 and M. Alexander all analyzed the data and wrote, edited, and revised the manuscript. All authors
515 approved the final version of the manuscript.

516

517 **Acknowledgements**

518 The authors wish to thank members of the Alexander lab including Jeffrey Fairley and Grace
519 Morrison for their assistance with experiments. The authors wish to thank Michael Lopez and
520 Anna Thalacker-Mercer for their critical evaluation of the manuscript prior to submission. The
521 authors wish to acknowledge Kirk Habegger, Shelly Nason, Jessica Antipenko, and members of
522 the UAB Diabetes Animal Physiology Core for assistance with the metabolic experiments. The
523 authors wish to acknowledge Mary Ballestas and Reid Millican from the UAB Neuroscience
524 NINDS Vector and Virus Core (Funded by NINDS P30 grant number NS047466). Research
525 reported in this publication was supported by Eunice Kennedy Shriver National Institute of Child
526 Health and Human Development, NIH, HHS of the National Institutes of Health under award
527 number R01HD095897 awarded to M.S. Alexander. M.S. Alexander is supported by an NIH Office
528 of Research Infrastructure Program (ORIP) U54 grant U54OD030167. A.S. was funded by a NIH
529 NINDS T32 training grant number 5T32NS095775.

530

531 **Figure Legend**
532
533 **Figure 1. Generation and validation of muscle-specific *Dock3* conditional knockout mice.**
534 **A.** Generation of *Dock3* mKO schematic. *Dock3*$^{fl/fl}$ mice containing two loxP sites flanking *Dock3*
535 exon 8 and 9 were mated with human-skeletal-actin (*HSA*)-*MerCreMer* mouse line to generate
536 the *Dock3* mKO mice. When administered tamoxifen (80 mg/kg) over five consecutive days this
537 induces a frameshift mutation resulting in a premature stop codon. **B.** PCR genotyping agarose
538 gel of *Dock3* heterozygous fl/+ alleles to produce homozygous flox/flox *Dock3* in skeletal muscle.
539 **C.** PCR genotyping agarose gel identifying loxP1 site (231 bp) and *Cre* recombinase (304 bp) in
540 *Dock3* flox/flox and WT mice (161 bp) mice in both tibialis anterior (TA) and whole brain lysates

541 (BR). **D.** Western blot of *Dock3* mKO mice indicating a reduction of protein as a result of ablation
542 of *Dock3*. **E.** Quantification of DOCK3 protein normalized to GAPDH loading control. **F.**
543 Immunofluorescent staining of adult TA muscles from the *Dock3*$^{fl/fl}$ and *Dock3* mKO mice for
544 LAMININ, DOCK3, and the merged image. Scale bar = 50 µm. **G.** Quantification of mean
545 fluorescence intensity (RFUs) in the *Dock3*$^{fl/fl}$ and *Dock3* mKO mice. Significance shown as ****p<
546 0.0001.
547
548 **Figure 2: Muscle-specific loss of *Dock3* results in a smaller myofiber sizes. A.** Hematoxylin
549 and eosin (H&E) stainings of TA muscles from *Dock3*$^{fl/fl}$ vs. *Dock3* mKO. Scale bar = 200 µm. **B.**
550 Quantification of myofiber diameters in *Dock3*$^{fl/fl}$ vs. *Dock3* mKO. Cross-sectional area shown as
551 frequency of fiber sizes over fiber size (µm^2).
552
553 **Figure 3. Loss of muscle *Dock3* reduces locomotor activity independent of physiological**
554 **force. A.** Schematic showing tamoxifen regimen for *Dock3*$^{fl/fl}$ and *Dock3* mKO. Mice were
555 administered an intraperitoneal injection of tamoxifen (80 mg/kg) for five consecutive days
556 followed by a three month washout period before assessing locomotor function. **B.** Activity
557 tracking traces in *Dock3*$^{fl/fl}$ vs. *Dock3* mKO mice. **C.** Quantification of total distance traveled (cm)
558 n = 9 mice/cohort, **D.** Quantification of mouse velocity, n = 9 mice/cohort, **E.** Force-frequency
559 relationship of EDL muscles from *Dock3* mKO vs. *Dock3*$^{fl/fl}$ EDL mice, n = 5 mice/cohort. **F.**
560 Inflection point of the force-frequency relationship (K) of EDL muscles from *Dock3* mKO vs.
561 *Dock3*$^{fl/fl}$ mice n = 5 mice/cohort. **G.** Slope of the force-frequency relationship (H) of EDL muscles
562 from *Dock3* mKO vs. *Dock3*$^{fl/fl}$ mice n = 5 mice/cohort. **H.** Peak force of EDL muscles from *Dock3*
563 mKO vs. *Dock3*$^{fl/fl}$ mice n = 5 mice/cohort. **I.** Peak force per physiological cross-sectional area
564 (CSA) of EDL muscles from *Dock3* mKO vs. *Dock3*$^{fl/fl}$ mice, n = 5 mice/cohort. **J.** Relative isometric
565 force measured during the eccentric contraction protocol for EDL muscles of *Dock3* mKO vs.
566 *Dock3*$^{fl/fl}$ mice, n = 5 mice/cohort. **K.** Relative force at the conclusion of the eccentric contraction
567 protocol for EDL muscles of *Dock3* mKO vs. *Dock3*$^{fl/fl}$ mice, n = 5 mice/cohort. The following p-
568 values of significance were stated: *p < 0.001, **p < 0.01, and ns = not significant.
569
570 **Figure 4. *Dock3* mKO mice show impaired skeletal muscle regeneration following injury.**
571 **A.** Schematic of cardiotoxin induced skeletal muscle TA injury. *Dock3* mKO mice and *Dock3*$^{fl/fl}$
572 mice were administered with an intramuscular injection of 10 µM of cardiotoxin at Day 0 and
573 sacrificed and harvested day 7 post-injury. **B.** Cross-section of injured tibialis anterior stained with
574 immunofluorescent antibody against LAMININ (green), DAPI (blue), and the merged image. Scale
575 bar = 200 µm. **C.** Quantification of immunofluorescent images from (**B**) analyzing % centralized
576 myonuclei per 600 fibers. **p < 0 .001, n = 4 mice/cohort. **D.** Masson's trichrome histochemical
577 analysis of injured TA in *Dock3*$^{fl/fl}$ vs. *Dock3* mKO 7 days post-injury. **E.** Quantification of
578 histochemical images from (**D**) with analysis of percent (%) fibrotic area in injured TA of *Dock3*$^{fl/fl}$
579 vs. *Dock3* mKO 7 days post-injury, n = 4 mice/cohort, p < 0.0001. Scale bar = 200 µm.
580
581 **Figure 5. *Dock3* mKO mice show increased body mass and whole body hyperglycemia. A.**
582 Quantitative magnetic resonance imaging indicated body weight differences between *Dock3*$^{fl/fl}$
583 and *Dock3* mKO mice, n = 10 mice/cohort, *p < 0.01. **B.** Quantitative magnetic resonance imaging
584 indicated differences in fat mass between *Dock3*$^{fl/fl}$ and *Dock3* mKO mice, n = 10 mice/cohort, *p
585 < 0.001. **C.** Quantitative magnetic resonance imaging indicating differences in lean mass between
586 *Dock3*$^{fl/fl}$ and *Dock3* mKO mice, n = 10 mice/cohort, ns = not significant. **D.** Glucose Tolerance
587 Test in *Dock3*$^{fl/fl}$ and *Dock3* mKO mice shown. Serum blood glucose level (mg/dl) measured over
588 time (minutes). **E.** Insulin Tolerance Test in *Dock3*$^{fl/fl}$ vs. *Dock3* mKO mice. n = 8 mice/cohort.
589 Serum blood glucose level (mg/dl) measured over time (minutes). **F.** WT and *Dock3* KO myoblasts
590 transfected with HA-GLUT-RFP. Wheat germ agglutinin stained membranes (green), GLUT4
591 (RFP), and nuclei are stained with DAPI. Scale bar = 10 µm.

592
593 **Figure 6. DOCK3 interacts with insulin signaling protein, SH3 domain-containing 1**
594 **(SORBS1). A.** DOCK3-SORBS1 yeast-2-hybrid neuromuscular cDNA screening library strategy.
595 **B.** Selection guide of DOCK3-SORBS1 yeast-2-hybrid amino acid selection. **C.** Positive
596 interaction of DOCK3-C-terminus and SORBS1 cDNA shown with yeast selective growth. **D.**
597 DOCK3-SORBS1 co-Immunoprecipitation in HEK293T cells. Immunoprecipitation (IP) performed
598 with DOCK3-GST and immunoblotting (IB) against SORBS-FLAG. **E.** GST-Pulldown domain
599 constructs shown indicating domains of full-length Dock3 and GST tagged PXXP motif. **F.**
600 DOCK3-SORBS1 GST-Pulldown immunoblots showing the interaction between recombinant
601 DOCK3 and SORBS1 directly interacting.
602
603 **Figure 7. DOCK3 interacts with SORBS1 via binding to the SORBS1 SH3 domains. A.**
604 Schematic showing the SORBS1 deletion constructs indicating full length SORBS1, and deletion
605 domains across each SH3 domain. **B.** The co-IP indicating the interaction and expression of each
606 deletion construct in HEK293T cells. **C.** The co-IP of DOCK3-SORBS1 in human primary
607 myoblasts. Immunoblot (DOCK3 rabbit polyclonal antibody) with the co-immunoprecipitation
608 (SORBS1-FLAG; FLAG mouse monoclonal antibody) **D.** The co-IP of SORBS1 deletion
609 constructs containing deletions of each of the SH3 domains in SORBS1 showing the requirements
610 for each in binding to DOCK3.
611

612 **References**

613 Aguet, F., S. Anand, K. G. Ardlie, S. Gabriel, G. A. Getz, A. Graubert, K. Hadley, R. E. Handsaker, K. H.
614 Huang, S. Kashin, X. Li, D. G. MacArthur, S. R. Meier, J. L. Nedzel, D. T. Nguyen, A. V. Segrè, E. Todres, B.
615 Balliu, A. N. Barbeira, A. Battle, R. Bonazzola, A. Brown, C. D. Brown, S. E. Castel, D. F. Conrad, D. J.
616 Cotter, N. Cox, S. Das, O. M. de Goede, E. T. Dermitzakis, J. Einson, B. E. Engelhardt, E. Eskin, T. Y. Eulalio,
617 N. M. Ferraro, E. D. Flynn, L. Fresard, E. R. Gamazon, D. Garrido-Martín, N. R. Gay, M. J. Gloudemans, R.
618 Guigó, A. R. Hame, Y. He, P. J. Hoffman, F. Hormozdiari, L. Hou, H. K. Im, B. Jo, S. Kasela, M. Kellis, S. Kim-
619 Hellmuth, A. Kwong, T. Lappalainen, X. Li, Y. Liang, S. Mangul, P. Mohammadi, S. B. Montgomery, M.
620 Muñoz-Aguirre, D. C. Nachun, A. B. Nobel, M. Oliva, Y. Park, Y. Park, P. Parsana, A. S. Rao, F. Reverter, J.
621 M. Rouhana, C. Sabatti, A. Saha, M. Stephens, B. E. Stranger, B. J. Strober, N. A. Teran, A. Viñuela, G.
622 Wang, X. Wen, F. Wright, V. Wucher, Y. Zou, P. G. Ferreira, G. Li, M. Melé, E. Yeger-Lotem, M. E. Barcus,
623 D. Bradbury, T. Krubit, J. A. McLean, L. Qi, K. Robinson, N. V. Roche, A. M. Smith, L. Sobin, D. E. Tabor, A.
624 Undale, J. Bridge, L. E. Brigham, B. A. Foster, B. M. Gillard, R. Hasz, M. Hunter, C. Johns, M. Johnson, E.
625 Karasik, G. Kopen, W. F. Leinweber, A. McDonald, M. T. Moser, K. Myer, K. D. Ramsey, B. Roe, S. Shad, J.
626 A. Thomas, G. Walters, M. Washington, J. Wheeler, S. D. Jewell, D. C. Rohrer, D. R. Valley, D. A. Davis, D.
627 C. Mash, P. A. Branton, L. K. Barker, H. M. Gardiner, M. Mosavel, L. A. Siminoff, P. Flicek, M. Haeussler, T.
628 Juettemann, W. J. Kent, C. M. Lee, C. C. Powell, K. R. Rosenbloom, M. Ruffier, D. Sheppard, K. Taylor, S. J.
629 Trevanion, D. R. Zerbino, N. S. Abell, J. Akey, L. Chen, K. Demanelis, J. A. Doherty, A. P. Feinberg, K. D.
630 Hansen, P. F. Hickey, F. Jasmine, L. Jiang, R. Kaul, M. G. Kibriya, J. B. Li, Q. Li, S. Lin, S. E. Linder, B. L.
631 Pierce, L. F. Rizzardi, A. D. Skol, K. S. Smith, M. Snyder, J. Stamatoyannopoulos, H. Tang, M. Wang, L. J.
632 Carithers, P. Guan, S. E. Koester, A. R. Little, H. M. Moore, C. R. Nierras, A. K. Rao, J. B. Vaught and S.
633 Volpi (2020). "The GTEx Consortium atlas of genetic regulatory effects across human tissues." Science
634 **369**(6509): 1318-1330.
635 Baumann, C. A., V. Ribon, M. Kanzaki, D. C. Thurmond, S. Mora, S. Shigematsu, P. E. Bickel, J. E. Pessin
636 and A. R. Saltiel (2000). "CAP defines a second signalling pathway required for insulin-stimulated glucose
637 transport." Nature **407**(6801): 202-207.

638 Beedle, A. M. (2016). "Cryosectioning of Contiguous Regions of a Single Mouse Skeletal Muscle for Gene
639 Expression and Histological Analyses." (118): e55058.
640 Bryan, B. A., D. Li, X. Wu and M. Liu (2005). "The Rho family of small GTPases: crucial regulators of
641 skeletal myogenesis." Cellular and Molecular Life Sciences CMLS **62**(14): 1547-1555.
642 Chaillou, T. and J. T. Lanner (2016). "Regulation of myogenesis and skeletal muscle regeneration: effects
643 of oxygen levels on satellite cell activity." The FASEB Journal **30**(12): 3929-3941.
644 Chang, T.-J., W.-C. Wang, C. A. Hsiung, C.-T. He, M.-W. Lin, W. H.-H. Sheu, Y.-C. Chang, T. Quertermous,
645 Y.-D. I. Chen, J. I. Rotter, L.-M. Chuang, C.-M. Hwu, Y.-J. Hung, W.-J. Lee, I. T. Lee and S. S. G. The (2018).
646 "Genetic variation of SORBS1 gene is associated with glucose homeostasis and age at onset of diabetes:
647 A SAPPHIRe Cohort Study." Scientific Reports **8**(1): 10574.
648 Chen, Q., C. A. Peto, G. D. Shelton, A. Mizisin, P. E. Sawchenko and D. Schubert (2009). "Loss of Modifier
649 of Cell Adhesion Reveals a Pathway Leading to Axonal Degeneration." The Journal of Neuroscience
650 **29**(1): 118-130.
651 Chiu, T. T., T. E. Jensen, L. Sylow, E. A. Richter and A. Klip (2011). "Rac1 signalling towards GLUT4/glucose
652 uptake in skeletal muscle." Cell Signal **23**(10): 1546-1554.
653 Côté, J.-F. and K. Vuori (2002). "Identification of an evolutionarily conserved superfamily of DOCK180-
654 related proteins with guanine nucleotide exchange activity." Journal of Cell Science **115**(24): 4901-4913.
655 DeFronzo, R. A. and D. Tripathy (2009). "Skeletal muscle insulin resistance is the primary defect in type 2
656 diabetes." Diabetes Care **32 Suppl 2**(Suppl 2): S157-163.
657 Gharaibeh, B., A. Lu, J. Tebbets, B. Zheng, J. Feduska, M. Crisan, B. Peault, J. Cummins and J. Huard
658 (2008). "Isolation of a slowly adhering cell fraction containing stem cells from murine skeletal muscle by
659 the preplate technique." Nat. Protocols **3**(9): 1501-1509.
660 Helbig, K. L., C. Mroske, D. Moorthy, S. A. Sajan and M. Velinov (2017). "Biallelic loss-of-function variants
661 in DOCK3 cause muscle hypotonia, ataxia, and intellectual disability." Clin Genet **92**(4): 430-433.
662 Helbig, K. L., C. Mroske, D. Moorthy, S. A. Sajan and M. Velinov (2017). "Biallelic loss-of-function variants
663 in DOCK3 cause muscle hypotonia, ataxia, and intellectual disability." Clinical Genetics: n/a-n/a.
664 Huntoon, V., J. J. Widrick, C. Sanchez, S. M. Rosen, C. Kutchukian, S. Cao, C. R. Pierson, X. Liu, M. A.
665 Perrella, A. H. Beggs, V. Jacquemond and P. B. Agrawal (2018). "SPEG-deficient skeletal muscles exhibit
666 abnormal triad and defective calcium handling." Human Molecular Genetics **27**(9): 1608-1617.
667 Iwata-Otsubo, A., A. L. Ritter, B. Weckselbatt, N. R. Ryan, D. Burgess, L. K. Conlin and K. Izumi (2018).
668 "DOCK3-related neurodevelopmental syndrome: Biallelic intragenic deletion of DOCK3 in a boy with
669 developmental delay and hypotonia." American Journal of Medical Genetics Part A **176**(1): 241-245.
670 Laurin, M., N. Fradet, A. Blangy, A. Hall, K. Vuori and J.-F. Côté (2008). "The atypical Rac activator
671 Dock180 (Dock1) regulates myoblast fusion in vivo." Proceedings of the National Academy of Sciences
672 **105**(40): 15446-15451.
673 Lesniewski, L. A., S. E. Hosch, J. G. Neels, C. de Luca, M. Pashmforoush, C. N. Lumeng, S. H. Chiang, M.
674 Scadeng, A. R. Saltiel and J. M. Olefsky (2007). "Bone marrow-specific Cap gene deletion protects against
675 high-fat diet-induced insulin resistance." Nat Med **13**(4): 455-462.
676 Li, J., X. Mi, L. Chen, G. Jiang, N. Wang, Y. Zhang, W. Deng, Z. Wang, G. Chen and X. Wang (2016). "Dock3
677 Participate in Epileptogenesis Through rac1 Pathway in Animal Models." Molecular Neurobiology **53**(4):
678 2715-2725.
679 Lim, C.-Y., X. Bi, D. Wu, J. B. Kim, P. W. Gunning, W. Hong and W. Han (2015). "Tropomodulin3 is a novel
680 Akt2 effector regulating insulin-stimulated GLUT4 exocytosis through cortical actin remodeling." Nature
681 Communications **6**(1): 5951.
682 Mandai, K., H. Nakanishi, A. Satoh, K. Takahashi, K. Satoh, H. Nishioka, A. Mizoguchi and Y. Takai (1999).
683 "Ponsin/SH3P12: an l-afadin- and vinculin-binding protein localized at cell-cell and cell-matrix adherens
684 junctions." J Cell Biol **144**(5): 1001-1017.

685 Moore, C. A., C. A. Parkin, Y. Bidet and P. W. Ingham (2007). "A role for the Myoblast city homologues
686 Dock1 and Dock5 and the adaptor proteins Crk and Crk-like in zebrafish myoblast fusion." Development
687 **134**(17): 3145-3153.
688 Mula, J., J. D. Lee, F. Liu, L. Yang and C. A. Peterson (2013). "Automated image analysis of skeletal muscle
689 fiber cross-sectional area." Journal of Applied Physiology **114**(1): 148-155.
690 Namekata, K., Y. Enokido, K. Iwasawa and H. Kimura (2004). "MOCA Induces Membrane Spreading by
691 Activating Rac1." Journal of Biological Chemistry **279**(14): 14331-14337.
692 Namekata, K., C. Harada, C. Taya, X. Guo, H. Kimura, L. F. Parada and T. Harada (2010). "Dock3 induces
693 axonal outgrowth by stimulating membrane recruitment of the WAVE complex." Proceedings of the
694 National Academy of Sciences **107**(16): 7586-7591.
695 Noviello, C., K. Kobon, L. Delivry, T. Guilbert, F. Julienne, P. Maire, V. Randrianarison-Huetz and A.
696 Sotiropoulos (2021). "RhoA within myofibers controls satellite cell microenvironment to allow
697 hypertrophic growth." bioRxiv: 2021.2001.2018.426685.
698 Raun, S. H., M. Ali, R. Kjøbsted, L. L. V. Møller, M. A. Federspiel, E. A. Richter, T. E. Jensen and L. Sylow
699 (2018). "Rac1 muscle knockout exacerbates the detrimental effect of high-fat diet on insulin-stimulated
700 muscle glucose uptake independently of Akt." The Journal of Physiology **596**(12): 2283-2299.
701 Reid, A. L., Y. Wang, A. Samani, R. M. Hightower, M. A. Lopez, S. R. Gilbert, L. Ianov, D. K. Crossman, L. J.
702 Dell'Italia, D. P. Millay, T. van Groen, G. V. Halade and M. S. Alexander (2020). "DOCK3 is a dosage-
703 sensitive regulator of skeletal muscle and Duchenne muscular dystrophy-associated pathologies."
704 Human Molecular Genetics **29**(17): 2855-2871.
705 Reid, A. L., Y. Wang, A. Samani, R. M. Hightower, M. A. Lopez, S. R. Gilbert, L. Ianov, D. K. Crossman, L. J.
706 Dell'Italia, D. P. Millay, T. van Groen, G. V. Halade and M. S. Alexander (2020). "“DOCK3 is a dosage-
707 sensitive regulator of skeletal muscle and Duchenne muscular dystrophy-associated pathologies”."
708 bioRxiv: 2020.2003.2027.010223.
709 Samani, A., K. G. English, M. A. Lopez, C. L. Birch, D. M. Brown, G. Kaur, E. A. Worthey and M. S.
710 Alexander (2022). "DOCKopathies: A systematic review of the clinical pathologies associated with human
711 DOCK pathogenic variants." Human Mutation **n/a**(n/a).
712 Sampath, S. C., S. C. Sampath and D. P. Millay (2018). "Myoblast fusion confusion: the resolution
713 begins." Skeletal Muscle **8**(1): 3.
714 Samson, T., C. Will, A. Knoblauch, L. Sharek, K. von der Mark, K. Burridge and V. Wixler (2007). "Def-6, a
715 guanine nucleotide exchange factor for Rac1, interacts with the skeletal muscle integrin chain alpha7A
716 and influences myoblast differentiation." J Biol Chem **282**(21): 15730-15742.
717 Schindelin, J., I. Arganda-Carreras, E. Frise, V. Kaynig, M. Longair, T. Pietzsch, S. Preibisch, C. Rueden, S.
718 Saalfeld, B. Schmid, J.-Y. Tinevez, D. J. White, V. Hartenstein, K. Eliceiri, P. Tomancak and A. Cardona
719 (2012). "Fiji: an open-source platform for biological-image analysis." Nature Methods **9**(7): 676-682.
720 Sylow, L., T. E. Jensen, M. Kleinert, J. R. Mouatt, S. J. Maarbjerg, J. Jeppesen, C. Prats, T. T. Chiu, S.
721 Boguslavsky, A. Klip, P. Schjerling and E. A. Richter (2013). "Rac1 Is a Novel Regulator of Contraction-
722 Stimulated Glucose Uptake in Skeletal Muscle." Diabetes **62**(4): 1139-1151.
723 Wang, Q., Z. Khayat, K. Kishi, Y. Ebina and A. Klip (1998). "GLUT4 translocation by insulin in intact muscle
724 cells: detection by a fast and quantitative assay." FEBS Letters **427**(2): 193-197.

725

Figure 1. Generation and validation of muscle-specific *Dock3* conditional knockout mice

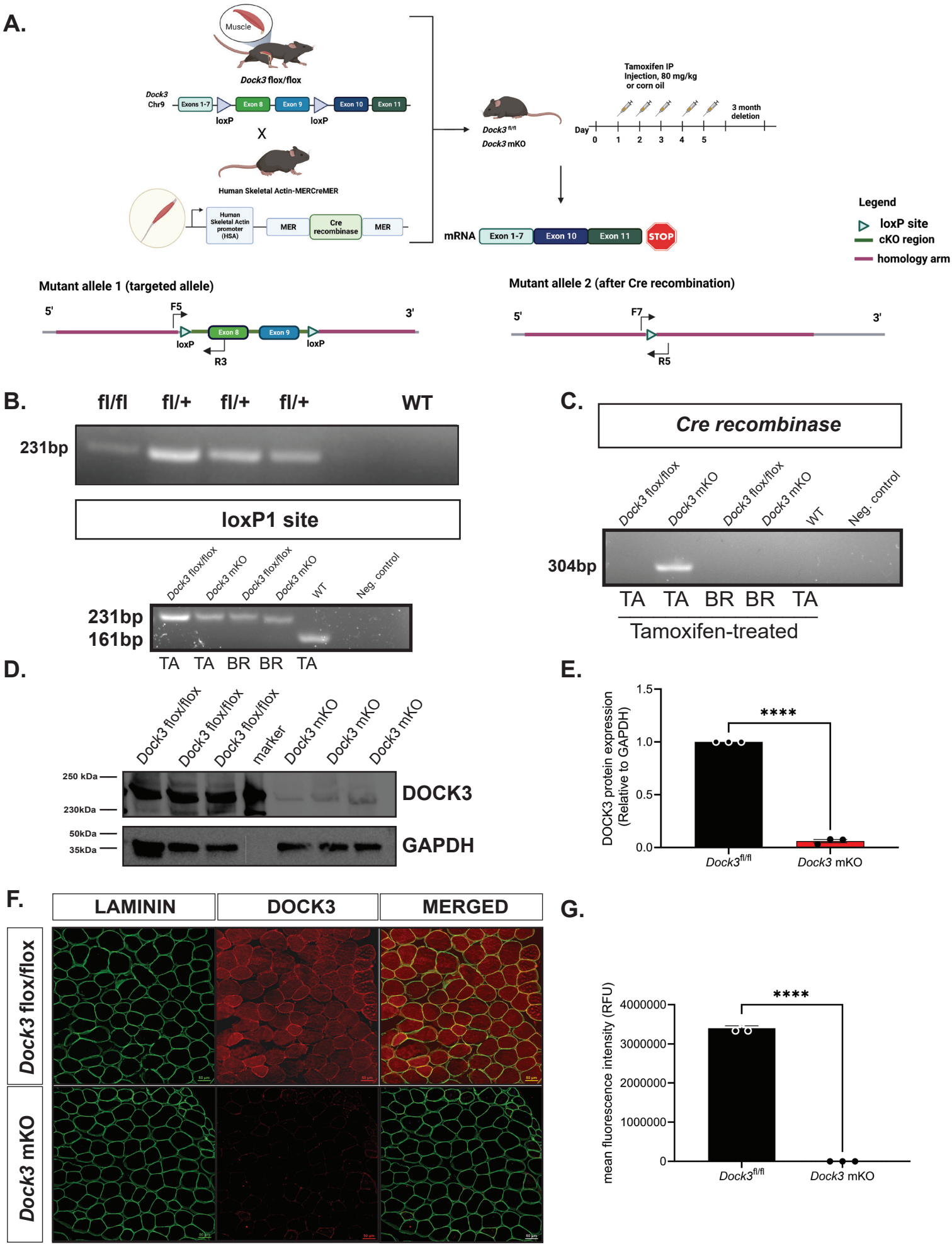

Figure 2. Muscle-specific loss of *Dock3* results in a smaller myofiber sizes

A.

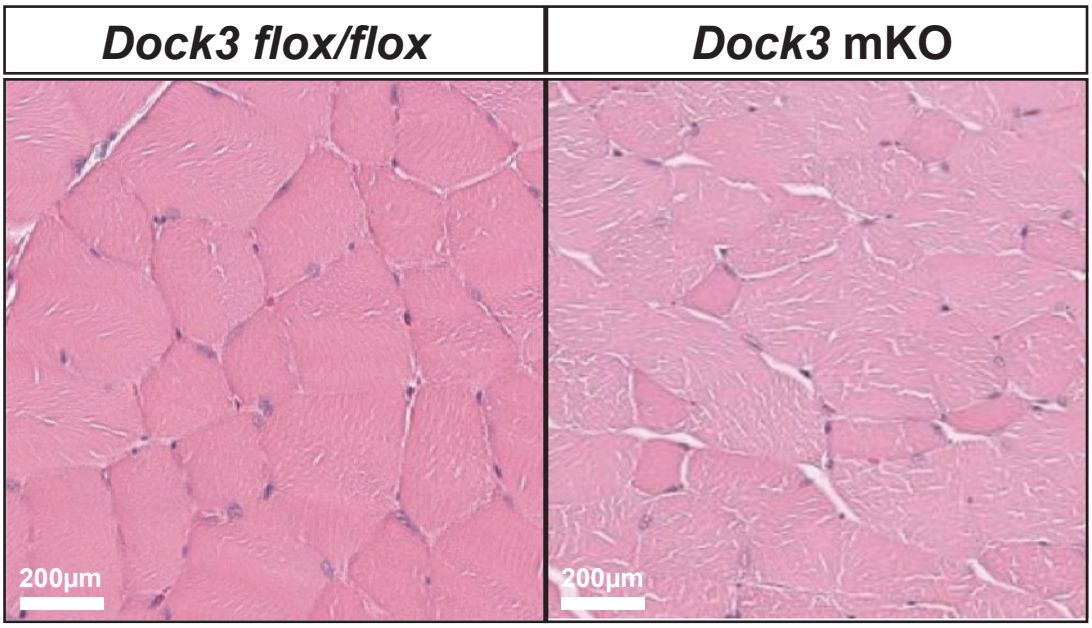

B.

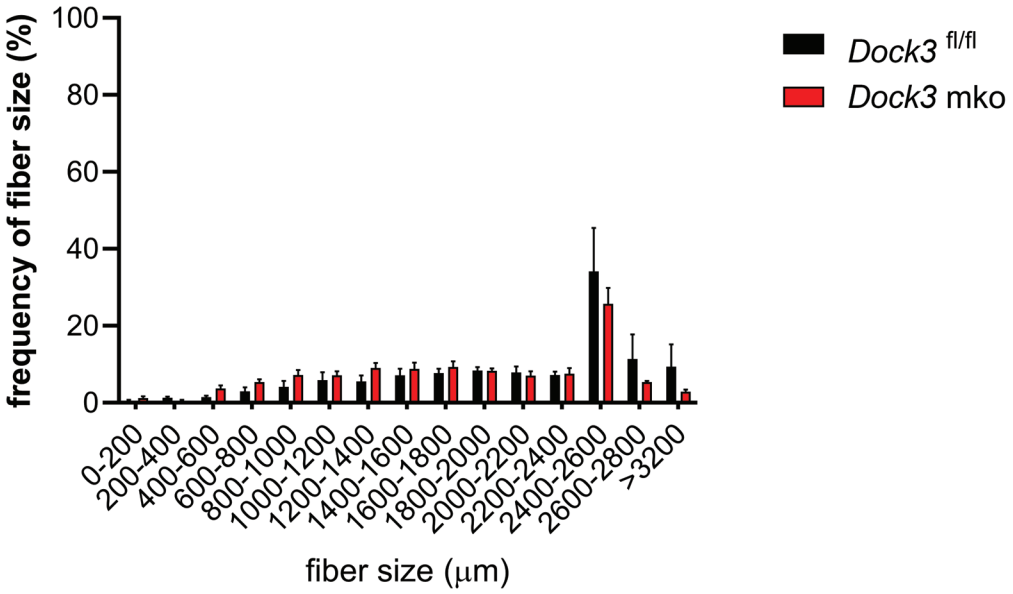

Figure 3. Loss of muscle *Dock3* reduces basal activity independent of physiological force

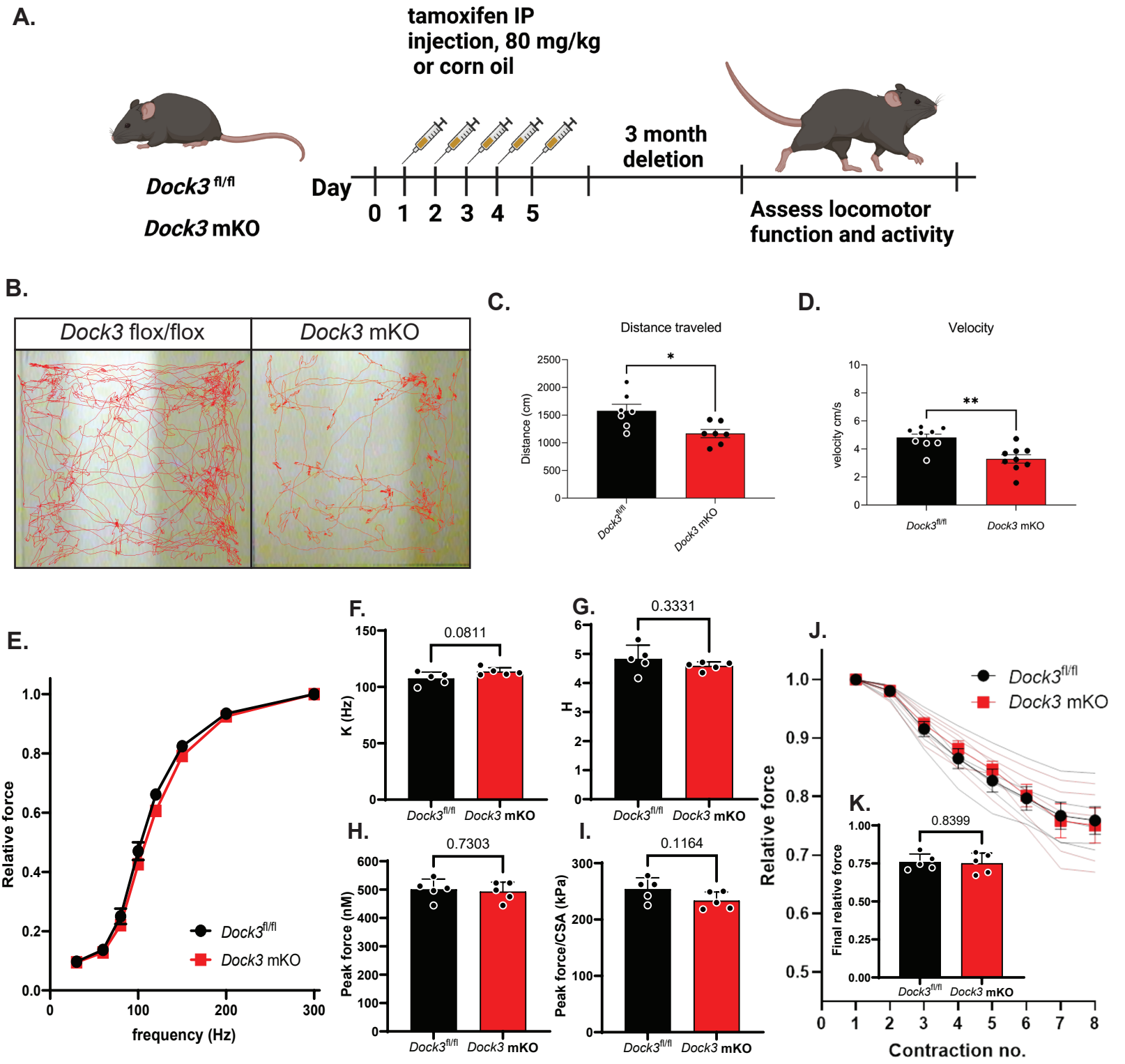

Figure 4. *Dock3* mKO mice show impaired skeletal muscle regeneration following injury

A.

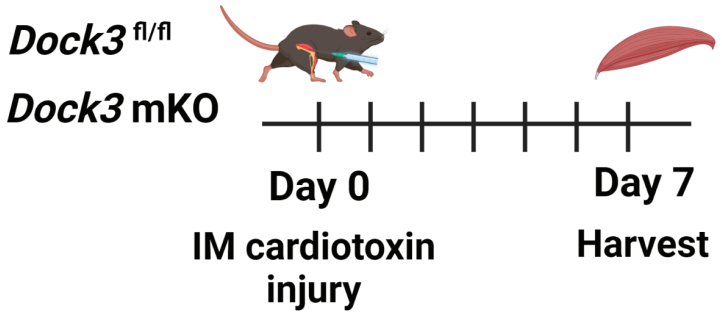

B.

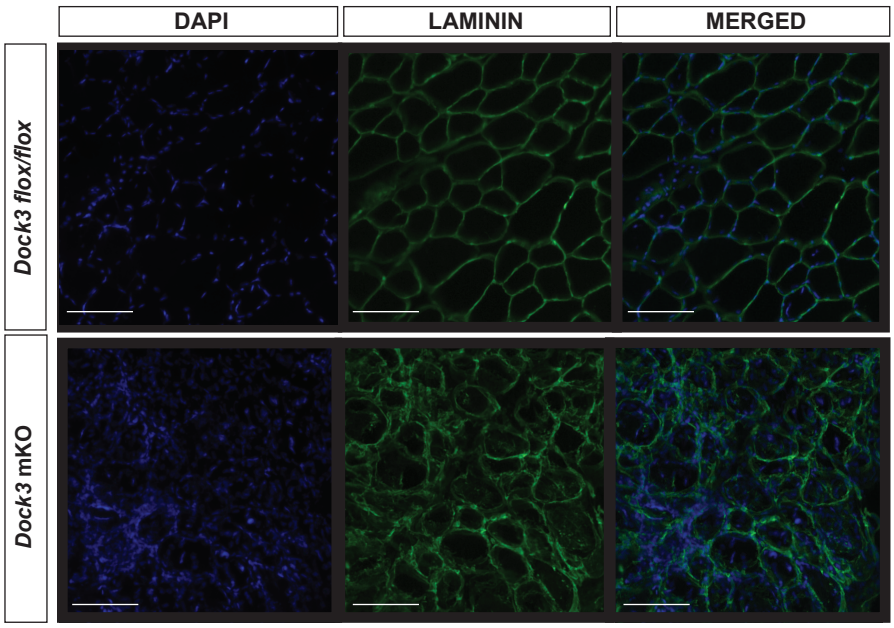

C.

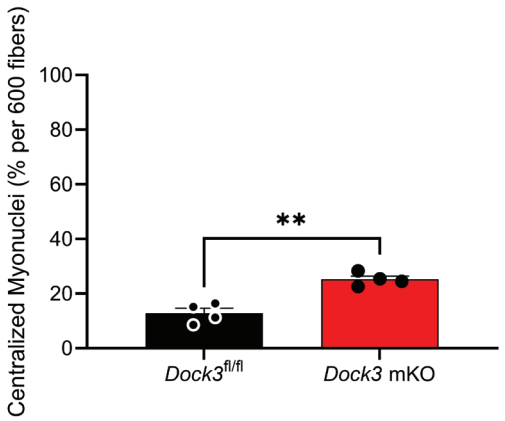

D.

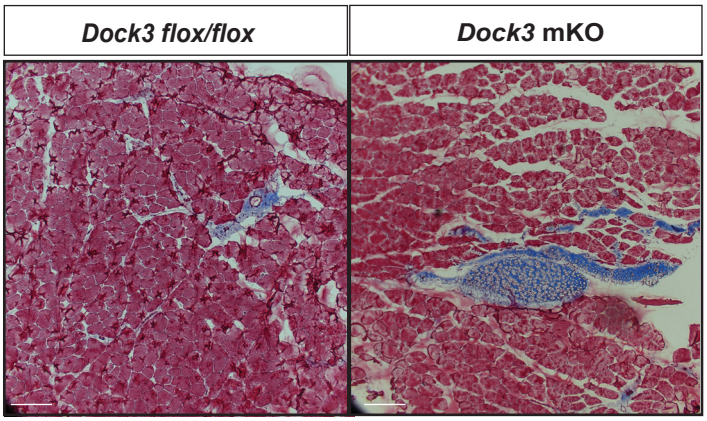

E.

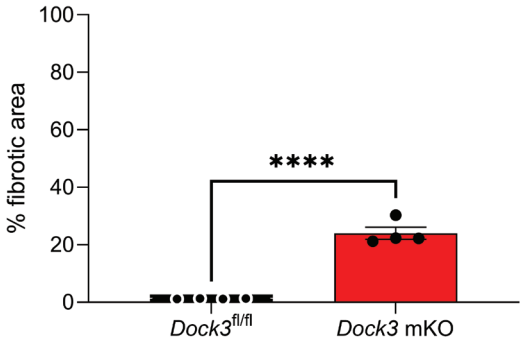

Figure 5. *Dock3* mKO mice show increased body mass and whole body hyperglycemia

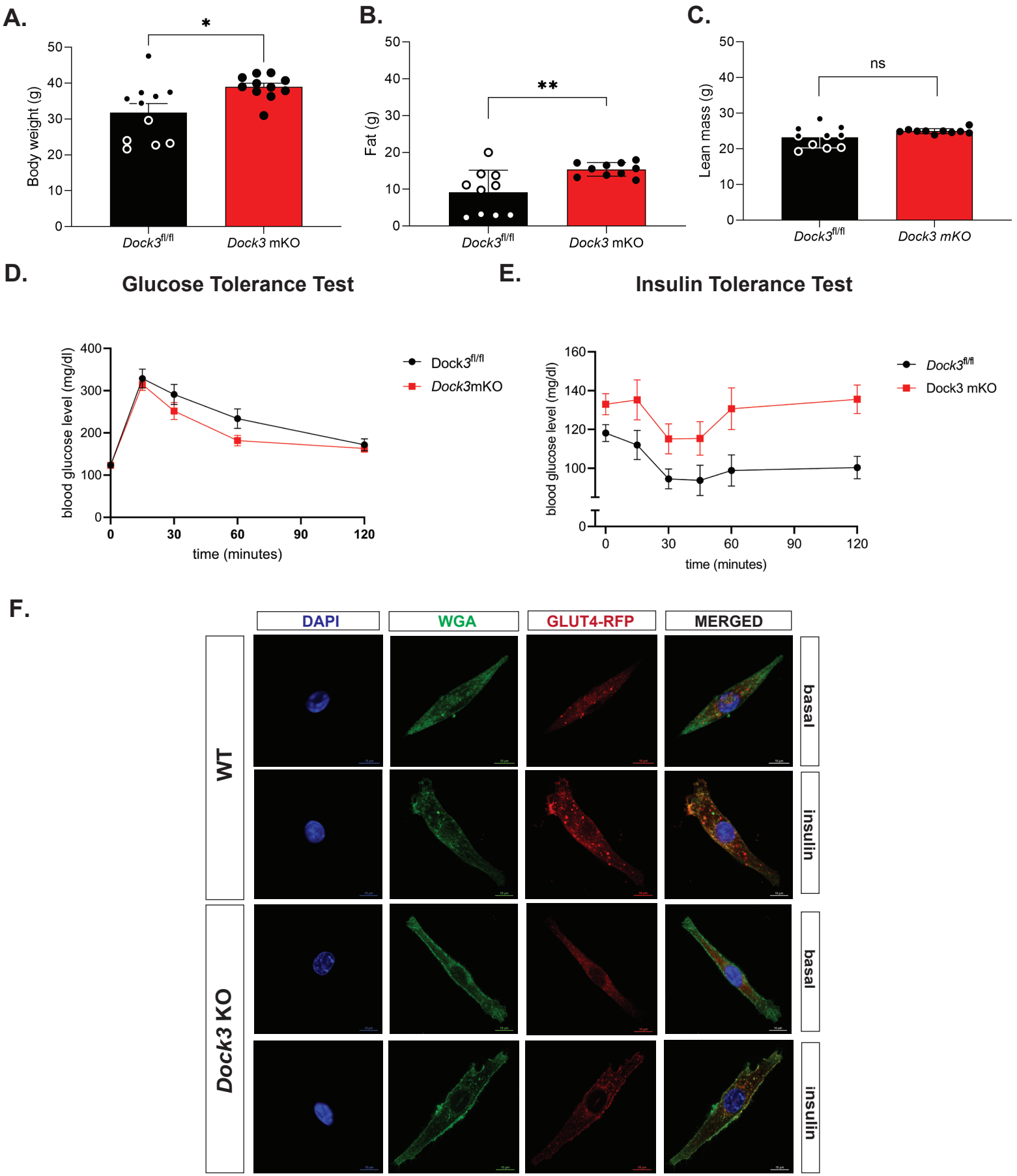

Figure 6. DOCK3 Interacts with insulin signaling protein, SH3 domain-containing 1 (SORBS1)

A.

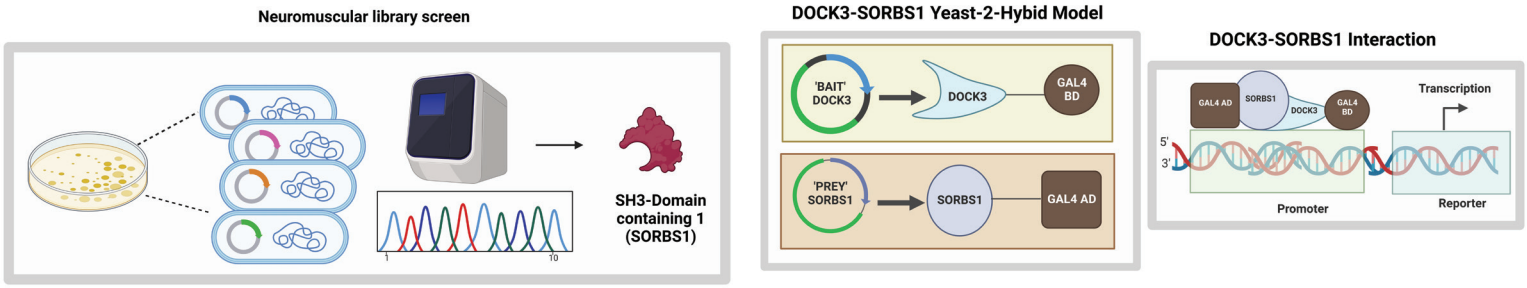

B.

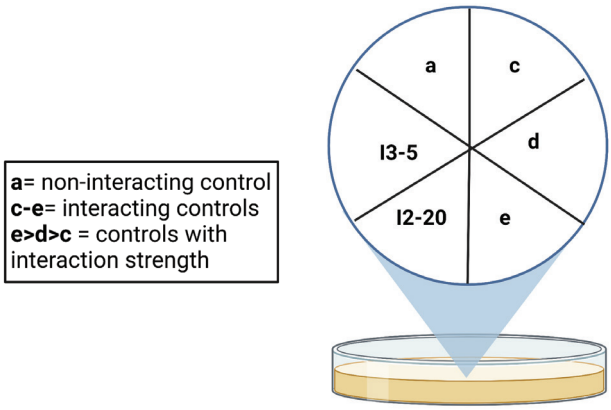

C.

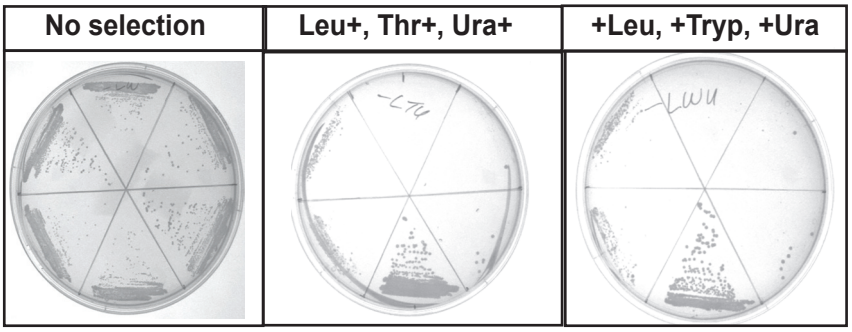

D. DOCK3-SORBS1 Co-Immunoprecipitation

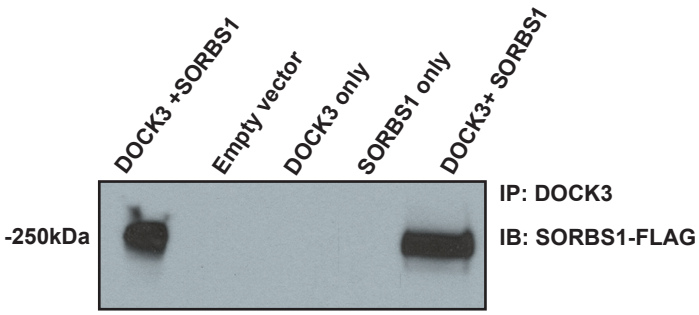

E.

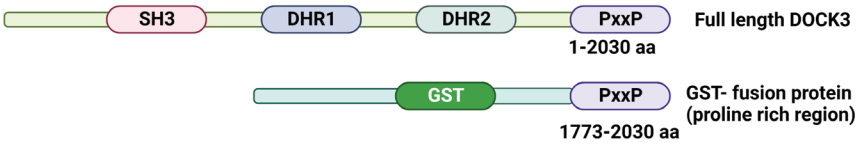

F. DOCK3-SORBS1 GST-Pulldown

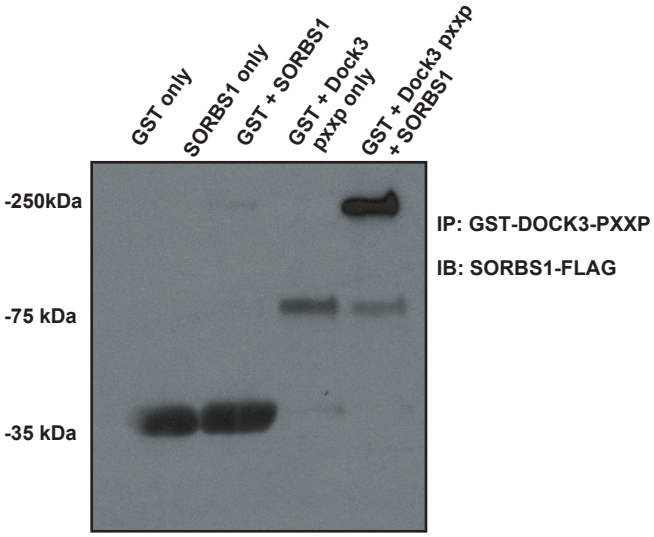
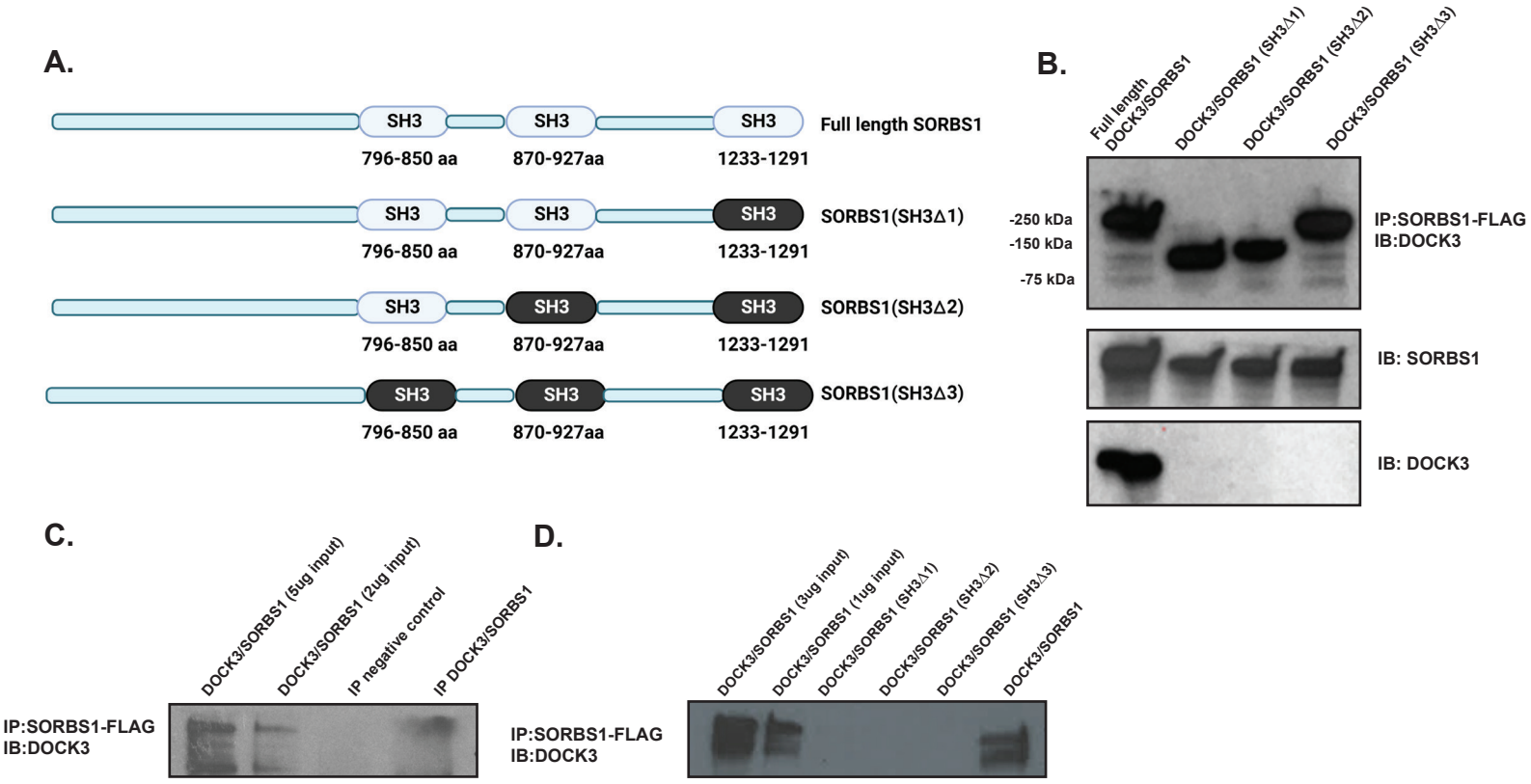
Figure 7. DOCK3 interacts with SORBS1 via binding to the SORBS1 SH3 domains